Pure Appl. Chem., Vol. 72, Nos. 1–2, pp. 281–291, 2000.

Localized-density-matrix method and its application to nanomaterials

GuanHua Chen, Satoshi Yokojima, WanZhen Liang, and XiuJun Wang

Department of Chemistry, The University of Hong Kong, Pokfulam Road, Hong Kong

Abstract: The localized-density-matrix (LDM) method has been developed to calculate the excited state properties of very large systems containing thousands of atoms. It is particularly suitable for simulating the dynamic electronic processes in nanoscale materials, and has been applied to poly(p-phenylenevynelene) (PPV) aggregates and carbon nanotubes. Absorption spectra of PPVs and carbon nanotubes have been calculated and compared to the experiments.

INTRODUCTION

With the development of modern technology, researchers may now synthesize and manipulate increasingly complex nanostructure materials. Nanomaterials contain hundreds or thousands of atoms, and have unique properties other than few atoms or macroscopic systems. Experiments like the scanning tunneling microscope (STM), atomic force microscope (AFM) and single molecule spectroscopy have provided a wealth of information on the nanomaterials, as well as posed many challenges to theory and computer simulation. Conventional *ab initio* and semiempirical molecular orbital calculations are usually limited to small and medium-size molecules. The obstacle lies in rapidly increasing computational costs as the systems become larger and more complex. The computational time t_{cpu} is proportional to a certain power of the system size, N^x, where N is the number of electronic orbitals involved, and x is an exponent which is usually larger than 2. For instance, the computational time of *ab initio* Hartree-Fock (HF) molecular orbital calculation has a O($N^{3–4}$) scaling, i.e., $x = 3 – 4$. To determine the electronic structures of very large systems, it is essential that the computational cost scales linearly with N. Several O(N) methods have been developed to calculate the electronic ground state [1–17]. The physical basis of these methods is "the nearsightedness of equilibrium systems" [8]. The excited states of very large electronic systems are much more difficult to determine. Several linear scaling calculations based on noninteracting electron models have been carried out to determine the excited state properties of large systems [9,18]. However, explicit inclusion of electronic correlation in the linear scaling calculation of the excited state properties has proven much more challenging.

A reduced single-electron density matrix ρ contains important information of an electronic system. Expressed in an orthonormal atomic orbital basis set, the diagonal element ρ_{ii} is the electron density at an atomic orbital i, and the off-diagonal element ρ_{ij} measures the electronic coherence between two atomic orbitals i and j. An equation of motion (EOM) for the reduced density matrix has been solved to calculate linear and nonlinear electronic responses to external fields [19,20]. This EOM is based on the time-dependent Hartree-Fock (TDHF) approximation, and the computational time for solving it scales as O(N^6) in the frequency domain and O(N^3) in the time domain. The TDHF approximation includes all single-electron excitations and partial double-, triple-, and other multi-electron excita-

Pure Appl. Chem.* **72, 1–331 (2000). An issue of reviews and research papers based on lectures presented at the 1st IUPAC Workshop on Advanced Materials (WAM1), Hong Kong, July 1999, on the theme of nanostructured systems.

tions. It has been applied successfully to investigate the optical properties of conjugated polymers. In ref. 21, it has been shown that the ground-state off-diagonal elements ρ_{ij} are negligible when the distance r_{ij} between i and j is larger than a critical length l_0. This is a consequence of "the nearsightedness of equilibrium systems". When the system is subjected to an external field $E(t)$, the field induces a change $\delta\rho$ in the reduced density matrix. The induced density matrix $\delta\rho$ has a similar "nearsightedness", i.e., off-diagonal element $\delta\rho_{ij}$ is approximately zero as the distance between i and j is large enough [21]. Different orders of responses in $E(t)$ have different critical lengths. Usually, the higher the order of response n is, the longer the critical length l_n is, i.e., $l_0 < l_1 < l_2 < l_3 \ldots$. We may truncate the nth order induced density matrix response $\delta\rho^{(n)}$ (note, $\delta\rho = \delta\rho^{(1)} + \delta\rho^{(2)} + \delta\rho^{(3)} + \ldots$) by setting its elements $\delta\rho_{ij}^{(n)}$ to zero if $r_{ij} > l_n$. This truncation may lead to a drastic reduction of the computational time.

Recently, a linear-scaling localized-density-matrix (LDM) method has been developed to evaluate the properties of excited states of very large electronic systems [22]. It is based on the TDHF approximation and the above mentioned truncation of reduced density matrix. Through the introduction of the critical lengths l_0, l_1, and others, which are characteristic of the reduced density matrices, the computational time of the LDM method scales linearly with the system size N. With the Pariser-Parr-Pople (PPP) Hamiltonian for the π electrons [23,24], the method has been tested successfully to evaluate the optical properties of polyacetylene oligomers containing up to 60 000 carbon atoms. Since the PPP model is applicable only to planar conjugated systems, the LDM method has been generalized to adopt the semiempirical models like CNDO/S [25] and PM3 [26] and was subsequently used to calculate the optical properties of carbon nanotubes and poly(p-phenylenevinylene) (PPV) aggregates. The LDM method is described in the section "Localized-density-matrix method". In the section "Polyacetylene", the calculations on polyacetyelene oligomers are presented and the scaling of the computational time versus the system size is examined. Applications to the PPV aggregates and carbon nanotubes are discussed in the sections "Poly(p-phenylenevinylene) aggregates" and "Carbon nanotubes", respectively.

LOCALIZED-DENSITY-MATRIX METHOD

There are three distinctive features of the LDM method [22]. First, instead of many-body wave functions, the reduced single-electron density matrix ρ is calculated from which the physical observables, such as the charge distribution, dipole moment, and photo-excitation spectrum, are determined. Since the expensive calculation of many-body wave function is avoided, the computational cost decreases substantially. Secondly, the reduced density matrix ρ is obtained by integrating the following Heisenberg equation,

$$i\hbar\dot{\rho}(t) = <[\mathbf{H}, \rho]> \tag{1}$$

in the time domain directly. Here $\rho \equiv <\rho>$, ρ is the reduced density matrix operator, and **H** is the Hamiltonian which may be that of PPP, CNDO/S, INDO/S, or PM3. Lastly, a truncation of ρ is adopted for its elements when the distance between the two atomic orbitals involved is beyond a critical length. This truncation reduces the number of reduced density matrix elements to be determined from N^2 to $O(N)$, where N is the number of the atomic orbitals in the system of interest, and leads subsquently to the linear-scaling of the computational time versus the system size.

The LDM method is a general method, and does not rely on specific approximation schemes. So far it has been implemented within the TDHF approximation [19]. In the TDHF approximation, a closed nonlinear self-consistent equation of motion (EOM) is yielded for the reduced single-electron density matrix $\rho(t)$

$$i\hbar\dot{\rho} = [h(t) + f(t), \rho(t)], \tag{2}$$

where $h(t)$ is the Fock matrix, and $f(t)$ represents the interaction between an electron and the external field $E(t)$. $\rho(t)$ and $h(t)$ may be decomposed as,

$$\rho(t) = \rho^{(0)} + \delta\rho(t), \tag{3}$$

$$h(t) = h^{(0)} + \delta h(t), \tag{4}$$

where $h^{(0)}$ and $p^{(0)}$ are respectively the Hartree-Fock ground-state reduced single-electron density matrix and Fock matrix, and $\delta\rho(t)$ and $\delta h(t)$ are the induced reduced density matrix and induced Fock matrix by the external field $E(t)$ respectively. Thus, Eq. 2 becomes

$$i\hbar\delta\dot{\rho} = [h^{(0)}, \delta\rho(t)] + [\delta h(t), \rho^{(0)}] + [f(t), \rho^{(0)}] + [\delta h(t), \delta\rho(t)] + [f(t), \delta\rho(t)]. \tag{5}$$

For the first order response,

$$i\hbar\delta\dot{\rho}_{ij}^{(1)} = \sum_k (h_{ik}^{(0)}\delta\rho_{kj}^{(1)} - \delta\rho_{ik}^{(1)}h_{kj}^{(0)}) + \sum_k (\delta h_{ik}^{(1)}\rho_{kj}^{(0)} - \rho_{ik}^{(0)}\delta h_{kj}^{(1)}) + \sum_k (f_{ik}\rho_{kj}^{(0)} - \rho_{ik}^{(0)}f_{kj}) \tag{6}$$

where k sums over all the atomic orbitals. Eq. 6 may be solved by integration in the time-domain. The following approximations

(a) $\rho_{ij}^{(0)} = 0$ if $r_{ij} > l_0$,

(b) $\delta\rho_{ij}^{(1)} = 0$ if $r_{ij} > l_1$

are the immediate consequence of the "nearsightedness" of the reduced density matrix, and lead directly to

(c) $h_{ij}^{(0)} = 0$ if $r_{ij} > l_0$,

(d) $\delta h_{ij}^{(1)} = 0$ if $r_{ij} > l_1$

With (a), (b), (c) and (d), the range of the summation $\sum_k$ is limited to a finite region for each term on the R.H.S. of Eq. 6. Thus, the computational cost for each $\delta\rho_{ij}^{(1)}$ is finite (i.e., not depending on N). Since only O(N) number of $\delta\rho_{ij}^{(1)}$ are to be determined [because of (b)], the total number of computational steps are then O(N) as well. The fast multipole method (FMM) or the cell multipole method (CMM) is employed to calculate h_{kk} and δh_{kk} [32–35]. This ensures the finite computational time for each h_{kk} and δh_{kk} and thus guarantee that the total computational time scales linearly with the system size. To calculate the nonlinear responses, the last two terms in Eq. 5 need to be included. The computational cost for evaluating these two terms scales linearly with N, and therefore, the O(N) scaling feature preserves for the calculation of higher order responses. It is emphasized that the LDM method is a general method, and does not rely on specific approximation, although the TDHF scheme has so far been adopted. To calculate the absorption spectrum, an external field

$$E(t) = \frac{1}{\sqrt{\pi\bar{t}}} e^{-(t/\bar{t})^2}, \tag{7}$$

is employed in the calculation where $\bar{t}$ determines the duration of the stimulating field.

To avoid unphysical results for the excited state properties, it is important that the relation [$h^{(0)}$, $\rho^{(0)}$] = 0 is satisfied to a high accuracy. A new linear-scaling procedure is to be devised to determine the

ground-state reduced density matrix $\rho^{(0)}$ [27]. To calculate $\rho^{(0)}$, we start with Eq. 2 by setting $E(t) = 0$, and have thus

$$i(\hbar d / dt + \gamma)\rho(t) = [h(t), \rho(t)] \tag{8}$$

where the damping coefficient γ is introduced to ensure the convergence of $\rho(t)$ to $\rho^{(0)}$. Starting from an initial guess to the ground state reduced density matrix, we may propagate $\rho(t)$ over a sufficient period of time until a convergence is reached, and the resulting ρ(t) may be taken as the ground-state reduced density matrix $\rho^{(0)}$.

POLYACETYLENE

To test its validity, we choose the polyacetylene (PA) oligomers and calculate their absorption spectra by employing the LDM method. The PPP Hamiltonian is used to describe the π electronic dynamics. Values of the parameters are the same as ref. 22.

The PPP Hartree-Fock ground-state density matrix $\rho^{(0)}$ must be calculated first. We plot the computational time to obtain $\rho^{(0)}$ in Fig. 1a. The computational time scales indeed linearly with the size N. The fourth-order Runge-Kutta method is used to integrate Eq. 2. A four-level hierarchy is used in the FMM calculation, and the smallest box contains 16 atoms. The absorption spectra of polyacetylene oligomers are calculated for N up to 60 000. In Fig. 1b, we plot the CPU time of the LDM calculation versus N. A time interval [–0.5 fs, –0.30 fs] with a time step 0.01 fs is used. The CPU time is indeed proportional to the system size N. In the calculations $l_0 = l_1 = 50$ Å, $t = 0.1$ fs, and the phenomenological dephasing constant γ is set to 0.1 eV. To access the accuracy of the LDM methods, the results for the full TDHF and the LDM methods are compared for $N = 200$, and are shown in Fig. 1c. Clearly two sets of results are consistent, which illustrates that the LDM method is highly accurate.

POLY(P-PHENYLENEVINYLENE) AGGREGATES

PPV-based materials possess high efficient electroluminescence, very large and ultrafast nonlinear optical responses, and favorable processing characteristics, and may thus be used for the fabrication of LEDs, photoconductors, optical switches and other devices. Much research activity has been devoted to investigating the nature of the excited states of these materials, and yet, many aspects of their photophysics remain controversial. For instance, one of many important issues is the intra- or inter-chain character of the photoexcitations [28–31]. Numerical simulations of optical responses that include explicit electron–electron correlation demand large computational resources, and have thus been limited mostly to single- and double-chain systems. It is thus vital to carry out reliable calculations to simulate the photoelectronic processes in bulk PPV-based materials. The LDM method is a linear-scaling method and applicable to the systems containing hundreds or thousands of atoms. We employ it to investigate the nature of inter- and intra-chain excitations. The PM3 Hamiltonian is adopted in the calculation.

We use the same bond lengths and angles of the PPV oligomer as given in ref. 36. The C–C bond lengths along the benzene ring are set to 1.39 Å, and all the angles on the benzene are set to 120°. The C–H bond lengths are equal to 1.09 Å. The single and double bond lengths in the vinylene group are 1.44 Å and 1.33 Å, respectively. To investigate the inter-chain excitations, we construct several PPV aggregates. Eight chain aggregates are shown in Fig. 2 where each chain is aligned along the x-axis and there are 3.28 Å and 1.64 Å displacements along x-direction from C to A and from B to A, respectively. The two PPV chains are either parallel (A and C) or tilted to each other with an angle 76° (A and B). The axis of B and C are displaced by (4.00 Å, 3.12 Å) and (–0.31 Å, 4.53 Å) in y-z plane from that of A. More chains are added with the same displacement vectors and angles among them, see Fig. 2. Each

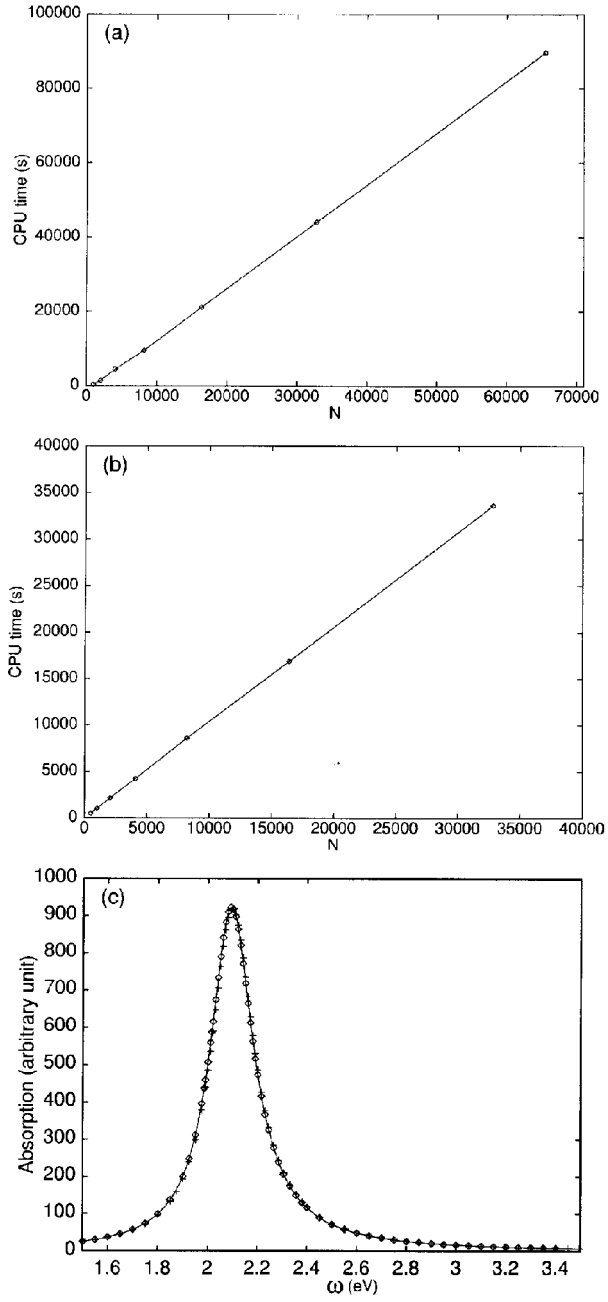

Fig. 1 (a) The CPU time versus N for the calculation of ground states reduced density matrices (l_1 = 50 Å and 16 atoms in the smallest box.) (b) The CPU time for the calculation of excited state ($l_1 = l_0$ = 37 Å and 16 atoms in the smallest box). Each calculation is performed during a time interval [–0.5 fs ,–0.3 fs] with a time step 0.01 fs. (c) The absorption spectrum for N = 200. The crosses are the cutoff-LDM results with $l_1 = l_0$ = 50 Å and l_c = 25 Å. The diamonds are the FMM-LDM results with $l_1 = l_0$ = 50 Å and 25 atoms in smallest box. The solid lines are the full TDHF results. Each calculation is performed during the time interval between –0.5 fs and 70.0 fs with a time step 0.01 fs. γ = 0.1 eV.

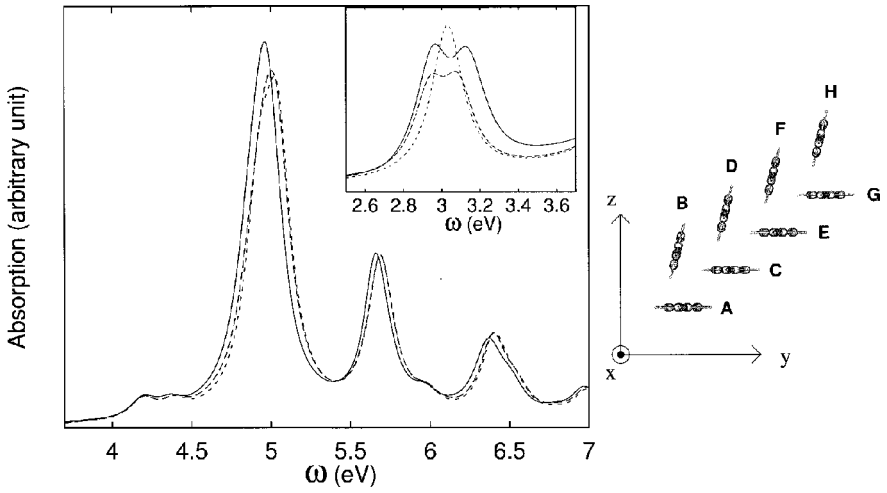

Fig. 2 Absorption spectra for 2-8 PPV aggregate. The solid line: 2-8 PPV aggregate. The dashed line: 2-2 PPV aggregate (A and B). The dotted line: 2-1 PPV oligomer (B). The dashed and dotted lines are magnified by 4 times. The inset shows the magnified view of the lower excited states. The electric field is perpendicular to the plane of A. $\gamma = 0.1$ eV.

PPV chain is made of multi-units and each unit consists of 8 carbon and 6 hydrogen atoms except the two ends of the chain. (The unit at either end of the chain has 8 carbon and 7 hydrogen atoms.) The notation *M-N* PPV represents a PPV aggregate containing *N* PPV chain and each chain having *M* units. The geometries are fixed in the calculation.

Figure 2 shows the comparison between the absorption spectra of 2-1 (chain C), 2-2 (A and B), and 2-8 (A to H) PPV aggregates. The electric field is perpendicular to the plane of A. The absorption spectra of 2-1 (dotted line) and 2-2 (dashed line) aggregates are scaled by a factor of 4. The change of the absorption spectra from one chain to two chains is again very small for higher energy except that the amplitude of the 2-8 absorption spectrum (solid line) is enhanced, and the peaks of 2-8 red shift compared to that of the 2-1. The first peak of 2-1 splits into two in 2-2 and larger splitting is observed in 2-8 PPV (see the inset of Fig. 2). This is the so-called Davydov splitting. A close look at the density matrices reveals that the two excitations that correspond to the splitting contain the inter-chain components. As the aggregate grows in size (from 2-1 to 2-2 to 2-8), the inter-chain component increases in the relative proportion of the density matrix. In other words, the inter-chain component becomes more important until it reaches about 20% as the size increases. All these effects come from the inter-chain excitations, which may be observed from the characteristics of corresponding density matrices.

The absorption spectra have been calculated for other PPV aggregates, and largest one so far has been the 8-4 aggregate which contains 464 atoms. In Fig. 3 we plot the absorption spectrum of the 4-4 PPV aggregate whose structure is sketched in the figure. The electronic field is polarized along the z-axis. Clearly, there is the Davydov splitting at $\omega \sim 2.7$ eV. Compared to those of the 2-4 and 2-8 PPV aggregates, the Davydov splitting red-shifts. It is because the longer the chain, the less the optical gap.

The inter-chain excitations become more prominent as the interaction amplitudes and channels increase. The precise features of the inter-chain excitations depends on the distance and interactions among the polymer chains in the aggregates. The relation between the photoluminescence and the inter-chain excitations or excimers is not yet clear, and more research is required.

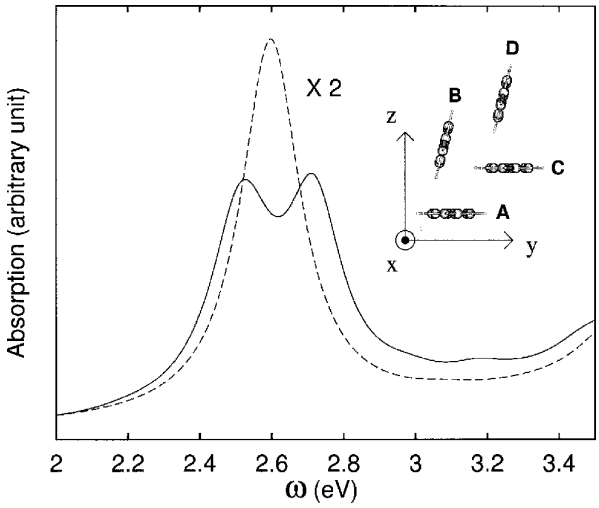

Fig. 3 Absorption spectra for 4-4 PPV aggregate. The solid line: 4-4 PPV aggregate. The doted line: 4-1 PPV oligomer (B). The dashed line is magnified by 4 times. The electric field is perpendicular to the plane of A. γ= 0.1 eV.

CARBON NANOTUBES

Carbon nanotubes (CNTs) have become a major subject of research activities since their initial finding by Iijima in 1991 [37] and the subsequent report for the synthesis of large quantities of CNTs by Ebbesen in 1992 [38]. CNTs may be metallic or semiconducting depending on their chiralities and the packing of the tubes. Because of their superior mechanical properties, CNTs have been widely used as the microscope probes. Tips of single-walled carbon nanotubes (SWNTs) and multi-walled CNTs (MWNTs) have been used in the atomic force microscope. Chemical functional groups have been added to the open ends of SWNTs. The resulting probes have distinctive chemical resolutions, and thus have been used in the newly developed chemical force microscope [39]. Our objective is to investigate the linear optical response of the zigzag CNTs by using the LDM method. The linear optical spectra of a series of open single-walled zigzag CNTs are evaluated. All the nearest-neighbor C-C distances $a_{c\text{-}c}$ are chosen to be 1.421 Å, which is the same as those in graphite. A tube diameter D_m is $\sqrt{3}ma_{c\text{-}c}/\pi$ in the zigzag (m,0) nanotubes which is formed by wrapping a graphite sheet along the zigzag direction (m,0) with m hexagons around the circumference. The PPP Hamiltonian is used in the calculation.

Figure 4a shows the absorption spectra of two (6,0) zigzag CNTs, $C_{384}H_{12}$ and $C_{768}H_{12}$. There is an apparent red-shift for the first peak of $C_{768}H_{12}$. Figure 4b shows the absorption spectra of two (9,0) zigzag CNTs, $C_{360}H_{18}$ and $C_{576}H_{18}$. Once again, the red-shift exists as the length of tube increases. The energy of first peak for either (6,0) or (9,0) depends on the length of the tube. The longer the tube, the smaller the first peak's energy. According to the tight binding model, (6,0) and (9,0) zigzag CNTs are metals while (7,0), (8,0) and other (3k ± 1,0) CNTs are semiconductors. In Fig. 5 we plot the absorption spectra for $C_{320}H_{16}$, $C_{512}H_{16}$ and $C_{1024}H_{16}$. The first peak for each CNT diminishes as the size increases and even disappears for $C_{1024}H_{16}$. As the size increases, the first major peak locates eventually at ω~1.9 eV, which is similar to the optical gap of polyacetylene. In the calculation the dephasing $\gamma$is set to 0.2 eV, and the critical lengths $l_0 = l_1$ =36 Å.

Carbon nanotubes are usually one-dimensional (1D) nanostructures since their lengths are far much larger than their diameters. In order to illustrate that the computational time of the LDM calcula-

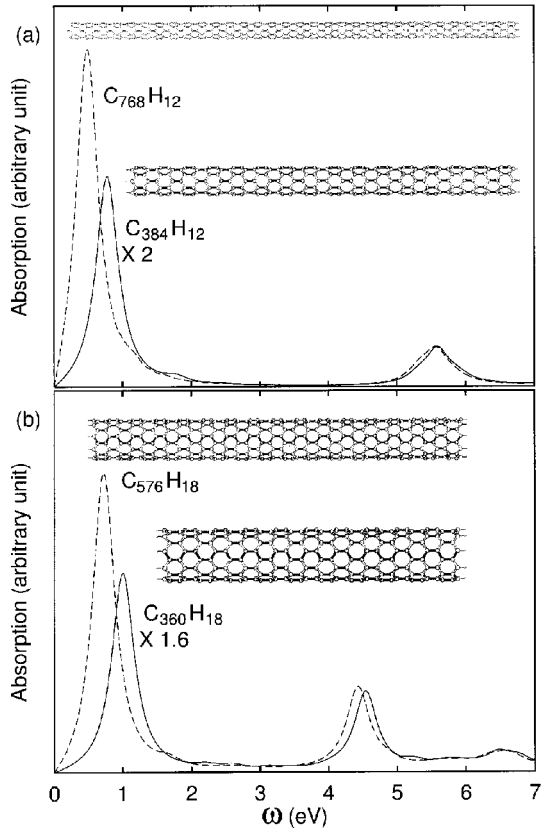

Fig. 4 Absorption spectra for zigzag CNTs. (a) (6,0): solid line is for $C_{384}H_{12}$ and dashed line for $C_{768}H_{12}$. (b) (9,0): solid line for $C_{360}H_{18}$, and dashed line for $C_{576}H_{18}$. The electric field is parallel to the tube. γ= 0.2 eV.

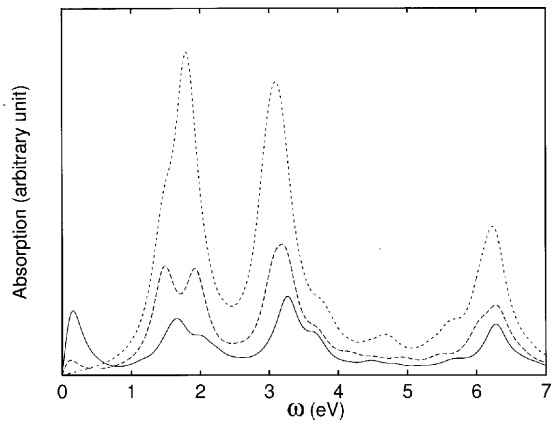

Fig. 5 The absorption spectra of the zigzag (8,0) CNTs. The dotted line for N=1024. The dashed line is for N = 512 , and the solid line is for N = 320. γ= 0.2 eV and $l_0 = l_1$ = 36 Å.

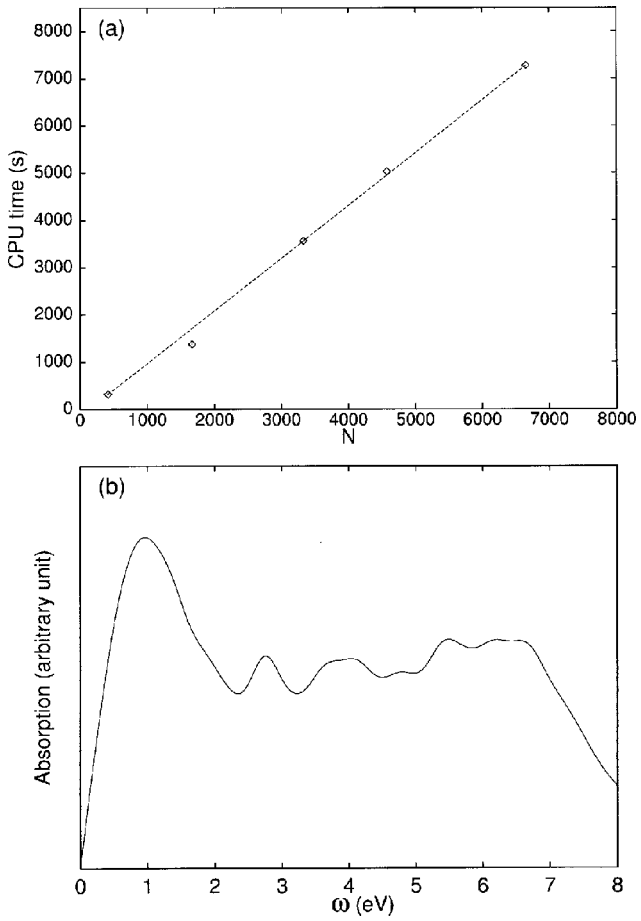

Fig. 6 (a) The CPU time for the excited state calculation of 3D CNTs with large radius. The time interval is [–0.5 fs, –0.3 fs] with the time step 0.01 fs. The critical lengths l_1 and l_0 are 15 Å. 26 atoms are included in the smallest box. (b) The absorption spectrum of the zigzag (60,0) nanotube $C_{1200}H_{120}$. γ= 0.4 eV.

tion scales linearly with the size for 2D and 3D systems, we construct the CNTs whose diameters are comparable to their lengths. The diameters range from 20.370 to 81.478 Å, and the lengths from 15.63 to 66.78 Å. The number of carbon atoms corresponds to 416, 1664, 3328, 4576, and 6656. The CPU time for propagating Eq. 2 between a time interval [–0.5 fs, –0.3 fs] is recorded. The time step is 0.01 fs. The results are shown in Fig. 6a. Clearly, the CPU time scales linearly with the system size *N*. The maximum number of atoms in the smallest box is kept to 26. As the diameter gets larger, the CNT is increasingly similar to the graphite. The absorption spectrum of a (60,0) CNT with 1200 carbon atoms is shown in Fig. 6b. The critical lengths l_0 = 28 and l_1 = 43 Å are used. The absorption spectrum is quite different with those of 1D CNTs. It should be similar to the optical properties of graphite if the tubule radius is large enough.

SUMMARY

It is demonstrated that the computational time of the LDM method scales linearly with the system size. The LDM method has been applied to the systems containing hundreds or thousands of atoms, and is

thus an ideal method for simulating electronic dynamics of nanoscale materials. Its applications to the PPV aggregates and carbon nanotubes have revealed interesting features of these materials, such as inter-chain excitations in the PPVs and low-frequency photoinduced excitations in the carbon nanotubes. The LDM method is applicable to many more nanomaterials and may become one of the major numerical methods for studying nanostructures.

ACKNOWLEDGEMENT

Support from the Hong Kong Research Grant Council (RGC) and the Committee for Research and Conference Grants (CRCG) of the University of Hong Kong is gratefully acknowledged.

REFERENCES

1. W. Yang. *Phys. Rev. Lett.* **66**, 1438 (1991); W. Yang and T. S. Lee. *J. Chem. Phys.* **103**, 5674 (1995).
2. X.-P. Li, R. W. Nunes, D. Vanderbilt. *Phys. Rev. B* **47**, 10891 (1993).
3. A. P. Cortona. *Phys. Rev. B* **44**, 8454 (1991).
4. G. Galli and M. Parrinello. *Phys. Rev. Lett.* **69**, 3547 (1992).
5. M. S. Daw. *Phys. Rev. B* **47**, 10895 (1993).
6. F. Mauri, G. Galli, R. Car. *Phys. Rev. B* **47**, 9973 (1993).
7. P. Ordejon, D. A. Drabold, M. P. Grumbach, R. M. Martin. *Phys. Rev. B* **48**, 14646 (1993).
8 . W. Kohn. *Chem. Phys. Lett.* **208**, 167 (1993); W. Kohn. *Phys. Rev. Lett.* **76**, 3168 (1996).
9. D. A. Drabold and O. F. Sankey. *Phys. Rev. Lett.* **70**, 3631 (1993).
10. M. Aoki. *Phys. Rev. Lett.* **71**, 3842 (1993).
11. B. Stechel, A. P. Williams, P. J. Feibelman. *Phys. Rev. B* **49**, 10088 (1994).
12. S. Goedecker and L. Colombo. *Phys. Rev. Lett.* **73**, 122 (1994).
13. J. P. Stewart. *Int. J. Quantum Chem.* **58**, 133 (1995).
14. M. C. Strain, G. E. Scuseria, M. J. Frisch. *Science* **271**, 51 (1996).
15. S. L. Dixon and K. M. Merz, Jr. *J. Chem. Phys.* **104**, 6643 (1996).
16. E. Schwegler, M. Challacombe, M. Head-Gordon *J. Chem. Phys.* **106**, 9708 (1997).
17. E. Hernandez and M. J. Gillan. *Phys. Rev. B* **51**, 10157 (1995).
18. T. Iitaka, S. Nomura, H. Hirayama, X. Zhao, Y. Aoyagi, T. Sugano. *Phys. Rev. E* **56**, 1222 (1997).
19. P. Ring and P. Schuck. *The Nuclear Many-Body Problem*, Springer, New York (1980).
20. A. Takahashi and S. Mukamel. *J. Chem. Phys.* **100**, 2366 (1994); G. H. Chen and S. Mukamel. *J. Am. Chem. Soc.* **117**, 4945 (1995).
21. G. H. Chen and S. Mukamel. *J. Phys. Chem.* **100**, 11080 (1996).
22. S. Yokojima and G. H. Chen. *Chem. Phys. Lett.* **292**, 379 (1998); S. Yokojima and G. H. Chen. *Phys. Rev. B* **59**, 7259 (1999); W. Z. Liang, S. Yokojima, G. H. Chen. *J. Chem. Phys.* **110**, 1844 (1999).
23. R. Pariser and R. G. Parr. *J. Chem. Phys.* **21**, 767 (1953).
24. J. A. Pople, Trans. Faraday Soc. **49**, 1375 (1953).
25. J. A. Pople, D. L. Beveridge, P. A. Dobosh. *J. Chem. Phys.* **47**, 2026 (1967); J. Ridley and M. Zerner. *Theor. Chim. Acta* **32**, 111 (1973). J. J. P. Stewart. *J. Comput. Chem.* **10**, 209 (1989).
26. M. J. S. Dewar and W. Thiel. *J. Am. Chem. Soc.* **99**, 4899 (1977); M. J. S. Dewar, E. G. Zoebisch, E. F. Healy, J. J. Stewart. *J. Am. Chem. Soc.* **107**, 3902 (1985).

27. S. Yokojima, D. H. Zhou, G. H. Chen. *Chem. Phys. Lett.* **302**, 495 (1999).
28. W. Graupner, J. Partee, J. Shinar, G. Leising, U. Scherf. *Phys. Rev. Lett.* **77**, 2033 (1996).
29. J. Grüner, P. J. Hamer, R. H. Friend, H.-J. Huber, U. Scherf, A. B. Holmes. *Adv. Mater.* **6**, 748 (1994).
30. S. A. Jenekhe and J. A. Osaheni. *Science* **265**, 765 (1994).
31. M. Yan, L. J. Rothberg, F. Papadimitrakopoulos, M. E. Galvin, T. M. Miller. *Phys. Rev. Lett.* **72**, 1104 (1994).
32. H. Q. Ding, N. Karasawa, W. A. Goddard III. *Chem. Phys. Lett.* **196**, 6 (1992).
33. H. Q. Ding, N. Karasawa, W. A. Goddard III. *J. Chem. Phys.* 97, 4309 (1992).
34. L. Greengard, V. J. Rokhlin. *Comput. Phys.* **73**, 325 (1987).
35. L. Greengard. *The Rapid Evaluation of Potential Fields in Particle Systems*, MIT Press: Cambridge, MA (1988).
36. P. Gomes da Costa, R. G. Dandrea, E. M. Conwell. *Phys. Rev. B* **47**, 1800 (1993).
37. S. Iijima. *Nature* **354**, 56 (1991).
38. T. W. Ebbesen and P. M. Ajayan. *Nature* **358**, 220 (1992).
39. S. S. Wong, A. T. Woolley, E. Joselevich, C. M., Lieber. *J. Am. Chem. Soc.* **120**, 8557 (1998).